INTERNATIONAL JOURNAL OF
NUMERICAL ANALYSIS AND MODELING
Volume 18, Number 2, Pages 143–164

NUMERICAL SIMULATIONS FOR SHALLOW WATER FLOWS OVER ERODIBLE BEDS BY CENTRAL DG METHODS

WEIZHI XIAN, AIMIN CHEN*, YONGPING CHENG, AND HAIYUN DONG

Abstract. In this paper, we investigate the shallow water flows over erodible beds by using a fully coupled mathematical model in two-dimensional space. This model combines the nonlinear shallow water equations, the sediment transport equation and the bed evolution equation. The purpose of this paper is to design a well-balanced and positivity-preserving scheme for this model. In order to achieve the well-balanced property, the coupled system is first reformulated as a new form by introducing an auxiliary variable. The central discontinuous Galerkin method is applied to discretize the model. By choosing the value of the auxiliary variable suitably, the scheme can exactly balance the flux gradients and source terms in the "still-water" case, and thus the well-balanced property of the proposed scheme can be proved. Moreover, the non-negativity of the volumetric sediment concentration in the sediment transport equation is maintained by choosing a suitable time step and using a positivity-preserving limiter. Numerical tests are presented to illustrate the validity of the proposed scheme.

Key words. Shallow water equation, sediment transport equation, bed evolution, central discontinuous Galerkin method, well-balanced and positivity-preserving scheme.

1. Introduction

The nonlinear shallow water (SW) equations over a fixed bed [17] are widely adopted to model free-surface flows in rivers, flood plains and coastal regions. However, the highly energetic flows over erodible beds may induce the sediment transport and the bed evolution. Therefore, the nonlinear SW equations over a fixed bed cannot accurately predict the motion of flows over erodible beds.

To overcome this issue, various hydraulics models have been presented to simulate the fluid flow and the sediment transport in the past decades. In 2002, Pritchard and Hogg [30] investigated the suspended sediment concentration by using the erosional and depositional models and reported the exact solution for the suspended sediment transport under one-dimensional (1D) dam-break flow. Cao et al. [3] investigated a 1D dam-break flow over mobile bed by considering the induced sediment transport and morphological evolution. In 2003, Fagherazzi and Sun [11] proposed a coupled model of the SW equations, the suspended sediment equation and the Exner equation in 1D case, which was used to simulate the initiation and evolution of transportational cyclic steps. In 2006, Simpson et al. [32] proposed a two-dimensional (2D) mathematical model based on the SW equations and empirical functions for bed friction, substrate erosion and deposition. This model is an extension of the 1D model in [3] and [11], and can be used to simulate the channel initiation and drainage basin evolution associated with overland flow and morphological changes induced by extreme events such as tsunami. In 2008, Abderrezzak et al. [1] proposed a 1D coupled model for dam-break waves over movable beds. This model is built on the shallow water equations, the Exner equation and a spatial lag equation. Based on the 1D model in [3], Yue et al. [39] developed a coupled

Received by the editors August 25, 2019 and, in revised form, January 19, 2021.
2000 *Mathematics Subject Classification.* 65M60, 65M12.

*Corresponding author.

mathematical model in 2D space, which comprises the shallow water equations and the empirical relationships for sediment exchange over erodible beds. In 2010, Xia et al. [35] presented a 2D model for predicting dam-break flows over mobile beds. In this model, they modified the shallow water equations, and thus the effects of sediment concentration and bed evolution can be considered during the flood wave propagation. These equations are combined with the non-equilibrium transport equations for graded sediments and the equation of bed evolution. Li et al. [24] proposed a fully coupled system to model the 2D SW equations with sediment mass conservation and bed topography evolution. In 2012, Hu et al. [13] employed a complete layer-averaged conservation laws, including the mass and momentum conservation equations for the watersediment mixture and mass conservation equations for sediment and bed material respectively. Besides the impact of the friction, the impacts of morphological change and water entrainment are also considered in their model. In 2015, Liu et al. [27] built a fully coupled system combining the 2D SW equations with friction terms and the 2D sediment transport equations for the total load and the morphological evolution equation. Besides the above works, many related works have also been proposed, see, e.g., [5, 6, 29, 34].

To solve the models related to the shallow water flows over erodible beds, many popular numerical schemes have been developed in the literature, such as the explicit finite difference scheme [1], the finite volume methods based on the Godunov-type scheme, the Roe-MUSCL scheme or the slope limited centred scheme [32, 35, 24, 13, 31], the Godunov-type central-upwind scheme [27] and the discontinuous Galerkin (DG) method [14, 33]. In [13] and [27], the authors investigated the well-balanced property of the numerical schemes. In [14], the authors considered the DG discretization of the evolution equation of the bed due to the transport of sediment, but they did not consider the shallow water equations and the volumetric sediment concentration. In [33], the authors investigated the DG discretization of the shallow water equations and the evolution of the bed, but they still did not consider the volumetric sediment concentration.

In this paper, we will consider the numerical simulation of shallow water flows over erodible beds, which are governed by a fully coupled 2D system of the shallow water equations, the volumetric sediment concentration and the bed evolution equation presented in [27]. The numerical method is based on the central DG method which is different from the DG method used in [14, 33]. The proposed method is still well-balanced and can maintain the non-negativity of the volumetric sediment concentration. For the purpose of numerics, the coupled system is first reformulated as a new form by introducing an auxiliary variable, which is easier to achieve the well-balanced property. The reformulation is similar to the one in [25] and is called as a "pre-balanced" form. In fact, the "pre-balanced" form in [25] is a special case when the auxiliary variable is zero in our reformulation.

In this paper, the central DG method, which is a variant of the DG method [9, 8, 28] and free of Riemann solvers, is applied to discretize the reformulated model. There are also other schemes which are free of Riemann solvers in the literature, such as the upwind central scheme [27]. Some numerical schemes with Riemann solvers use a bound or a approximation value of the maximum eigenvalue [16]. The central DG method is also one of popular high order numerical methods, which was originally presented by Liu and his collaborators [26]. A well-balanced central DG method coupling with the finite element method was employed to solve the 1D fully nonlinear weakly dispersive Green-Naghdi model over varying topography ([21]). A positivity-preserving well-balanced central DG method was developed for solving the shallow water equations ([22]).

The central DG method doubles the degrees of freedom in comparison to a conventional DG method, but no Riemann solvers are needed, thus the computational efficiency is a significant topic. A previous work in [10] has compared the efficiency between the central DG method and the DG method, the authors reported that the central DG method is more time-consuming in comparison to the DG method, thus they proposed a reconstructed central DG method to improve the efficiency. This method can be applied to improve the computing efficiency of the proposed method in the present work. The reconstructed central DG method is comparable to the standard DG method and is directly compatible with the procedures to ensure well-balancedness and non-negativity of the volumetric sediment concentration [7]. For more works on the central DG method, see, e.g., [19, 18, 23, 38, 20].

In order to preserve the "still-water" solution, a special value of the auxiliary variable is chosen, and then we can prove the well-balanced property of the presented scheme. Since the central DG method uses two overlapping meshes and the numerical solutions is discontinuous across the edge of cell, the auxiliary variable cannot be set as zero as in [25]. Moreover, the non-negativity of the volumetric sediment concentration in the sediment transport equations is maintained by choosing suitable time step and using a positivity-preserving limiter. The non-negativity is also proved in this paper. The CFL condition in the positivity-preserving scheme is different from the one in [22, 37] due to a source term appearing in the volumetric sediment concentration equation. It is a trivial work to combine the positivity-preserving scheme for the water depth [22] into the proposed scheme, thus it is not considered in this paper.

The remainder of the paper is organized as follows. In Section 2, we introduce the mathematical model studied in this paper. Then, we present the numerical method for the model and discuss the well-balanced property of the scheme and the non-negativity of the volumetric sediment concentration in Section 3. Section 4 shows a range of numerical tests to illustrate the reliability of the proposed method. Finally, concluding remarks are given in Section 5.

2. Mathematical model

In this paper, we consider a fully coupled shallow water model which is used to simulate flows over erodible beds in 2D space [27]

$$h_t + (hu)_x + (hv)_y = -b_t, \tag{1}$$

$$(hu)_t + (hu^2 + 0.5gh^2)_x + (huv)_y = -gh(b_x + f_1), \tag{2}$$

$$(hv)_t + (huv)_x + (hv^2 + 0.5gh^2)_y = -gh(b_y + f_2), \tag{3}$$

$$(hc)_t + (huc)_x + (hvc)_y = E - M, \tag{4}$$

$$b_t + \frac{\mu}{1-p}(u(u^2+v^2))_x + \frac{\mu}{1-p}(v(u^2+v^2))_y = \frac{M-E}{1-p}. \tag{5}$$

Herein, the subscripts t, x and y represent the partial derivative with respect to the time variable and the space variables, respectively. h denotes the water depth, u and v are the vertically averaged horizontal velocity in the x- and y-directions, respectively, c represents the volumetric sediment concentration and b is the bed. p denotes the bed porosity, g represents the gravitational constant and μ is a coefficient related to the grain diameter and the kinematic viscosity of the sediment mixture. f_1 and f_2 are friction slope terms in the x- and y-directions, respectively, which are evaluated by

$$f_1 = n_b^2 u\sqrt{u^2+v^2}/h^{4/3}, \quad f_2 = n_b^2 v\sqrt{u^2+v^2}/h^{4/3} \tag{6}$$

with n_b being the Manning's roughness coefficient. Throughout of this paper, we always assume the water depth $h \geq h_0 > 0$. Therefore, equation (6) is well-defined.

In equations (4)-(5), E denotes the bed sediment entrainment due to turbulence and M represents the sediment deposition due to gravity, which are two distinct mechanisms involved in the sediment exchange and bed evolution processes. We follow [27] to calculate E and M:

$$M = w_0(1-Z_a)^m Z_a, \tag{7}$$

$$E = \begin{cases} \frac{\phi(\gamma-\gamma_c)\sqrt{u^2+v^2}}{hd^{1/5}} & \text{if } \gamma \geq \gamma_c, \\ 0 & \text{otherwise,} \end{cases} \tag{8}$$

$$\gamma = h\sqrt{f_1^2+f_2^2}/(sd) \tag{9}$$

$$w_0 = \sqrt{(13.95\nu/d)^2 + 1.09sgd} - 13.95\nu/d, \tag{10}$$

$$Z_a = \alpha c, \alpha = \min\{2, (1-p)/c\} \tag{11}$$

where ν is the kinematic viscosity of water, d is the average diameter of sediment particles and $s = \rho_s/\rho_f - 1$ is the submerged specific gravity of sediment with ρ_s denoting the density of sediment particles and ρ_f being the density of clear water, m is an exponent indicating the effects of hindered settling due to high sediment concentration, Z_a is the local near-bed sediment concentration in volume. ϕ is a positive coefficient to control the erosion force, γ is the dimensionless shear stress, and γ_c is the critical Shields parameter for initiation of sediment movement. The values of the parameters $g, \mu, p, n_b, d, \nu, \rho_s, \rho_f, \gamma_c$ will be given in numerical tests.

In order to present the numerical scheme more conveniently, we define $\eta = h + b, q_1 = hu, q_2 = hv, r = hc$ and rewrite the equations (1)- (5) in the following vector form:

$$\mathbf{U}_t + \mathbf{F}(\mathbf{U})_x + \mathbf{G}(\mathbf{U})_y = \mathbf{S}(\mathbf{U}) \ , \tag{12}$$

where

$$\mathbf{U} = (\eta, q_1, q_2, r, b)^\top , \tag{13}$$

$$\mathbf{F}(\mathbf{U}) = \left(q_1, \frac{q_1^2}{\eta-b} + \frac{1}{2}g(\eta-b)^2, \frac{q_1q_2}{\eta-b}, \frac{q_1 r}{\eta-b}, \frac{\mu}{1-p}\frac{q_1\left(q_1^2+q_2^2\right)}{(\eta-b)^3}\right)^\top , \tag{14}$$

$$\mathbf{G}(\mathbf{U}) = \left(q_2, \frac{q_1q_2}{\eta-b}, \frac{q_2^2}{\eta-b} + \frac{1}{2}g(\eta-b)^2, \frac{q_2 r}{\eta-b}, \frac{\mu}{1-p}\frac{q_2\left(q_1^2+q_2^2\right)}{(\eta-b)^3}\right)^\top , \tag{15}$$

$$\mathbf{S}(\mathbf{U}) = \left(0, -g(\eta-b)\left(b_x+f_1\right), -g(\eta-b)\left(b_y+f_2\right), E-M, \frac{M-E}{1-p}\right)^\top . \tag{16}$$

3. Numerical schemes

In this section, we develop the numerical method for the solution of the fully coupled shallow water model over erodible beds. The proposed method preserves the "still-water" solution and maintains the non-negativity of the volumetric sediment concentration.

3.1. Notations. In this paper, we adopt the notations in [22]. Let $\{x_{i-\frac{1}{2}}\}_i$ and $\{y_{j-\frac{1}{2}}\}_j$ denote the partitions of $[x_{\min}, x_{\max}]$ and $[y_{\min}, y_{\max}]$, respectively. Define $x_i = \frac{1}{2}(x_{i-\frac{1}{2}} + x_{i+\frac{1}{2}})$, $y_j = \frac{1}{2}(y_{j-\frac{1}{2}} + y_{j+\frac{1}{2}})$, $C_{ij} = [x_{i-\frac{1}{2}}, x_{i+\frac{1}{2}}] \times [y_{j-\frac{1}{2}}, y_{j+\frac{1}{2}}]$ and $D_{ij} = [x_{i-1}, x_i] \times [y_{j-1}, y_j]$. Thus $\mathcal{T}_h^C = \{C_{ij}, \forall i, j\}$ and $\mathcal{T}_h^D = \{D_{ij}, \forall i, j\}$ are two overlapping meshes for the computational domain $\Omega = [x_{\min}, x_{\max}] \times [y_{\min}, y_{\max}]$. On the two meshes, we can define the following discrete spaces

$$
\begin{aligned}
\mathcal{W}_n^{C,k} &= \{\mathbf{v} = (v_1, v_2, ..., v_n)^\top : v_l|_{C_{ij}} \in P^k(C_{ij}), l = 1, 2, ..., n, \forall i, j\} \ , \\
\mathcal{W}_n^{D,k} &= \{\mathbf{v} = (v_1, v_2, ..., v_n)^\top : v_l|_{D_{ij}} \in P^k(D_{ij}), l = 1, 2, ..., n, \forall i, j\} \ ,
\end{aligned}
$$

where n is a positive integer. $P^k(C_{ij})$ denotes the space of polynomials in C_{ij} with degree of at most k.

We denote the Legendre Gauss-Lobatto quadrature points on $[x_{i-\frac{1}{2}}, x_i]$, $[x_i, x_{i+\frac{1}{2}}]$, $[y_{j-\frac{1}{2}},\ y_j]$ and $[y_j, y_{j+\frac{1}{2}}]$ by $\widehat{L}_i^{1,x} = \{\widehat{x}_i^{1,\beta}, \beta = 1, 2, \ldots, \widehat{N}\}$, $\widehat{L}_i^{2,x} = \{\widehat{x}_i^{2,\beta}, \beta = 1, 2, \ldots, \widehat{N}\}$, $\widehat{L}_j^{1,y} = \{\widehat{y}_j^{1,\gamma}, \gamma = 1, 2, \ldots, \widehat{N}\}$ and $\widehat{L}_j^{2,y} = \{\widehat{y}_j^{2,\gamma}, \gamma = 1, 2, \ldots, \widehat{N}\}$, respectively. We denote the corresponding quadrature weights on the reference element $[-\frac{1}{2}, \frac{1}{2}]$ by $\{\widehat{\omega}_\beta, \beta = 1, 2, \ldots, \widehat{N}\}$, in which $\widehat{N}$ is chosen such that $2\widehat{N} - 3 \geq k$. We denote the Gaussian quadrature points on $[x_{i-\frac{1}{2}}, x_i]$, $[x_i, x_{i+\frac{1}{2}}]$, $[y_{j-\frac{1}{2}}, y_j]$ and $[y_j, y_{j+\frac{1}{2}}]$ by $L_i^{1,x} = \{x_i^{1,\beta}, \beta = 1, 2, \ldots, N\}$, and $L_i^{2,x} = \{x_i^{2,\beta}, \beta = 1, 2, \ldots, N\}$, $L_j^{1,y} = \{y_j^{1,\gamma}, \gamma = 1, 2, \ldots, N\}$ and $L_j^{2,y} = \{y_j^{2,\gamma}, \gamma = 1, 2, \ldots, N\}$, respectively. We denote the corresponding quadrature weights on the interval $[-\frac{1}{2}, \frac{1}{2}]$ by $\{\omega_\beta, \beta = 1, 2, \ldots, N\}$, in which N is chosen such that the Gaussian quadrature is exact for the integration of univariate polynomials of degree $2k + 1$. Then we define $L_{i,j}^{l,m} = (L_i^{l,x} \otimes L_j^{m,y}) \cup (L_i^{l,x} \otimes \widehat{L}_j^{m,y}) \cup (\widehat{L}_i^{l,x} \otimes L_j^{m,y})$ with $l, m = 1, 2$. The points in $L_{i,j}^{l,m}, l, m = 1, 2$ are also shown in Figure 1.

The proposed scheme evolves two copies of numerical solutions, which are denoted by $\mathbf{U}^{n,\star} = (\eta^{n,\star}, q_1^{n,\star}, q_2^{n,\star}, r^{n,\star}, b^{n,\star})^\top \in \mathcal{W}^\star$, $\star = C, D$, at t_n.

3.2. Standard central DG method. In this subsection, we use the standard central DG method [26] for space discretization and the forward Euler method for time discretization to solve (12). That is to find $\mathbf{U}^{n+1,C} \in \mathcal{W}_5^{C,k}$ and $\mathbf{U}^{n+1,D} \in \mathcal{W}_5^{D,k}$ such that $\forall\ \mathbf{V}^C \in \mathcal{W}_5^{C,k}, \forall\ \mathbf{V}^D \in \mathcal{W}_5^{D,k}$,

$$
\begin{aligned}
\int_{C_{ij}} \mathbf{U}^{n+1,C} \cdot \mathbf{V}^C dxdy &= \int_{C_{ij}} \left(\theta \mathbf{U}^{n,D} + (1-\theta)\mathbf{U}^{n,C}\right) \cdot \mathbf{V}^C dxdy \\
&+ \Delta t_n \int_{C_{ij}} \left[\mathbf{F}\left(\mathbf{U}^{n,D}\right) \cdot \mathbf{V}_x^C + \mathbf{G}\left(\mathbf{U}^{n,D}\right) \cdot \mathbf{V}_y^C\right] dxdy \\
&- \Delta t_n \int_{y_{j-\frac{1}{2}}}^{y_{j+\frac{1}{2}}} \Big[\mathbf{F}\left(\mathbf{U}^{n,D}\left(x_{i+\frac{1}{2}}, y\right)\right) \cdot \mathbf{V}^C\left(x_{i+\frac{1}{2}}^-, y\right) \\
&- \mathbf{F}\left(\mathbf{U}^{n,D}(x_{i-\frac{1}{2}}, y)\right) \cdot \mathbf{V}^C\left(x_{i-\frac{1}{2}}^+, y\right)\Big] dy \\
&- \Delta t_n \int_{x_{i-\frac{1}{2}}}^{x_{i+\frac{1}{2}}} \Big[\mathbf{G}\left(\mathbf{U}^{n,D}\left(x, y_{j+\frac{1}{2}}\right)\right) \cdot \mathbf{V}^C\left(x, y_{j+\frac{1}{2}}^-\right) \\
&- \mathbf{G}\left(\mathbf{U}^{n,D}\left(x, y_{j-\frac{1}{2}}\right)\right) \cdot \mathbf{V}^C\left(x, y_{j-\frac{1}{2}}^+\right)\Big] dx \\
&+ \Delta t_n \int_{C_{ij}} \mathbf{S}\left(\mathbf{U}^{n,D}\right) \cdot \mathbf{V}^C dxdy \ , \qquad (17)
\end{aligned}
$$

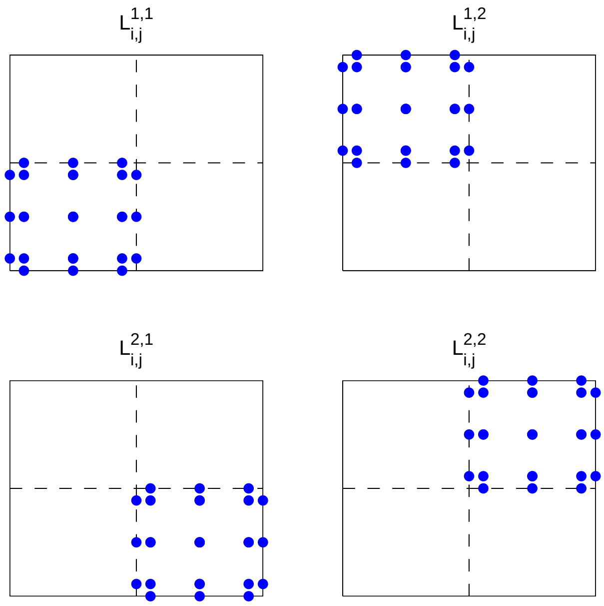

FIGURE 1. The points in $L_{i,j}^{l,m}, l, m = 1, 2$ located in the cell C_{ij}.

$$
\begin{aligned}
\int_{D_{ij}} \mathbf{U}^{n+1,D} \cdot \mathbf{V}^D dxdy \;=\;& \int_{D_{ij}} \left(\theta \mathbf{U}^{n,C} + (1-\theta)\mathbf{U}^{n,D}\right) \cdot \mathbf{V}^D dxdy \\
&+ \Delta t_n \int_{D_{ij}} \left[\mathbf{F}\left(\mathbf{U}^{n,C}\right) \cdot \mathbf{V}_x^D + \mathbf{G}\left(\mathbf{U}^{n,C}\right) \cdot \mathbf{V}_y^D\right] dxdy \\
&- \Delta t_n \int_{y_{j-1}}^{y_j} \left[\mathbf{F}\left(\mathbf{U}^{n,C}\left(x_i, y\right)\right) \cdot \mathbf{V}^D\left(x_i^-, y\right)\right. \\
&- \left.\mathbf{F}\left(\mathbf{U}^{n,C}(x_{i-1}, y)\right) \cdot \mathbf{V}^D\left(x_{i-1}^+, y\right)\right] dy \\
&- \Delta t_n \int_{x_{i-1}}^{x_i} \left[\mathbf{G}\left(\mathbf{U}^{n,C}\left(x, y_j\right)\right) \cdot \mathbf{V}^D\left(x, y_j^-\right)\right. \\
&- \left.\mathbf{G}\left(\mathbf{U}^{n,C}\left(x, y_{j-1}\right)\right) \cdot \mathbf{V}^D\left(x, y_{j-1}^+\right)\right] dx \\
&+ \Delta t_n \int_{D_{ij}} \mathbf{S}\left(\mathbf{U}^{n,C}\right) \cdot \mathbf{V}^D dxdy\ , \qquad (18)
\end{aligned}
$$

where Δt_n is the time step and $\theta \in [0, 1]$ is a constant. Notice that the scheme given by (17)-(18) is not a well-balanced scheme, namely, it does not satisfy the "still-water" solution exactly

$$\eta = h + b = C_0 \text{ (Constant)}, u = v = 0. \qquad (19)$$

Since both variables $r = hc$ and b may be the functions of time while the identities in (19) hold, they are different from the case of the classical nonlinear SW equations where b is independent of time. Therefore,it is a challenging work to design a well-balanced scheme that satisfies (19) exactly when the initial data satisfies (19).

3.3. Well-balanced central DG method. In this subsection, we present a well-balanced scheme based on the standard central DG method for the system (12). In [22], the authors proposed a positivity-preserving well-balanced central DG method for the nonlinear shallow water equations over fixed beds. The well-balanced property of the scheme is achieved by adding modification terms to the discretization scheme. While in this work, to achieve the well-balanced property, the coupled model is first reformulated as a new form by introducing an auxiliary variable. By choosing the value of the auxiliary variable suitably, the central DG scheme can exactly balance the flux gradients and source terms in the "still-water" case. There is no modification terms added in the discretization scheme.

We reformulate the system (12) as the following form

$$\mathbf{U}_t + \tilde{\mathbf{F}}(\mathbf{U}, A)_x + \tilde{\mathbf{G}}(\mathbf{U}, A)_y = \tilde{\mathbf{S}}(\mathbf{U}, A) \ , \tag{20}$$

where

$$\tilde{\mathbf{F}}(\mathbf{U}, A) = \left(q_1, \frac{q_1^2}{\eta - b} + \frac{1}{2} g\eta^2 - g(\eta - A)b, \frac{q_1 q_2}{\eta - b}, \frac{q_1 r}{\eta - b}, \frac{\mu}{1-p}\frac{q_1\left(q_1^2 + q_2^2\right)}{(\eta - b)^3} \right)^\top , \tag{21}$$

$$\tilde{\mathbf{G}}(\mathbf{U}, A) = \left(q_2, \frac{q_1 q_2}{\eta - b}, \frac{q_2^2}{\eta - b} + \frac{1}{2} g\eta^2 - g(\eta - A)b, \frac{q_2 r}{\eta - b}, \frac{\mu}{1-p}\frac{q_2\left(q_1^2 + q_2^2\right)}{(\eta - b)^3} \right)^\top , \tag{22}$$

$$\tilde{\mathbf{S}}(\mathbf{U}, A) = \left(0, -g(\eta - A)b_x - ghf_1, -g(\eta - A)b_y - ghf_2, E - M, \frac{M - E}{1-p} \right)^\top , \tag{23}$$

where A is constant or a variable only dependent on time t. Equation (20) is a "pre-balanced" formulation of the shallow water system (12). This formulation will greatly simplify the achievement of the well-balanced property of the proposed scheme.

The standard central DG method can be applied to the new system (20). That is to find $\mathbf{U}^{n+1,C} \in \mathcal{W}_5^{C,k}$ such that $\forall\ \mathbf{V} \in \mathcal{W}_5^{C,k}$,

$$\begin{aligned}
\int_{C_{ij}} \mathbf{U}^{n+1,C} \cdot \mathbf{V} dxdy \ &= \ \int_{C_{ij}} \left(\theta \mathbf{U}^{n,D} + (1-\theta)\mathbf{U}^{n,C} \right) \cdot \mathbf{V} dxdy \\
&+ \ \Delta t_n \int_{C_{ij}} \left[\tilde{\mathbf{F}}\left(\mathbf{U}^{n,D}, A^{n,D}\right) \cdot \mathbf{V}_x + \tilde{\mathbf{G}}\left(\mathbf{U}^{n,D}, A^{n,D}\right) \cdot \mathbf{V}_y \right] dxdy \\
&- \ \Delta t_n \int_{y_{j-\frac{1}{2}}}^{y_{j+\frac{1}{2}}} \left[\tilde{\mathbf{F}}\left(\mathbf{U}^{n,D}\left(x_{i+\frac{1}{2}}, y\right), A^{n,D}\right) \cdot \mathbf{V}\left(x_{i+\frac{1}{2}}^-, y\right) \right. \\
&- \ \left. \tilde{\mathbf{F}}\left(\mathbf{U}^{n,D}(x_{i-\frac{1}{2}}, y), A^{n,D}\right) \cdot \mathbf{V}\left(x_{i-\frac{1}{2}}^+, y\right) \right] dy \\
&- \ \Delta t_n \int_{x_{i-\frac{1}{2}}}^{x_{i+\frac{1}{2}}} \left[\tilde{\mathbf{G}}\left(\mathbf{U}^{n,D}\left(x, y_{j+\frac{1}{2}}\right), A^{n,D}\right) \cdot \mathbf{V}\left(x, y_{j+\frac{1}{2}}^-\right) \right. \\
&- \ \left. \tilde{\mathbf{G}}\left(\mathbf{U}^{n,D}\left(x, y_{j-\frac{1}{2}}\right), A^{n,D}\right) \cdot \mathbf{V}\left(x, y_{j-\frac{1}{2}}^+\right) \right] dx \\
&+ \ \Delta t_n \int_{C_{ij}} \tilde{\mathbf{S}}\left(\mathbf{U}^{n,D}, A^{n,D}\right) \cdot \mathbf{V} dxdy \ .
\end{aligned} \tag{24}$$

The procedure to update $\mathbf{U}^{n+1,D}$ is similar to (18), thus it is omitted. In the well-balanced scheme, the value of $A^{n,D}$ is significant in the case of the "still-water" solution.

In particular, it should be a constant equal to the same value of the water surface η at initial time. Therefore, in this work $A^{n,D}$ is defined by

$$A^{n,D} = \frac{1}{|\Omega|}\int_\Omega \eta^{n,D} dxdy \ . \tag{25}$$

Theorem 1. *The proposed numerical method defined in* (24)-(25)*, and its counterpart for* $\mathbf{U}^{n+1,D}$*, to solve the fully coupled shallow water model over erodible beds* (12)*, is a well-balanced scheme. That is to say, the scheme preserves the "still-water" solution* (19)*.*

Proof. : Let

$$\hat{\mathbf{U}} = (\eta, q_1, q_2)^\top \ , \tag{26}$$

$$\hat{\mathbf{F}}(\mathbf{U}, A) = \left(q_1, \frac{q_1^2}{\eta - b} + \frac{1}{2}g\eta^2 - g(\eta - A)b, \frac{q_1 q_2}{\eta - b}\right)^\top \ , \tag{27}$$

$$\hat{\mathbf{G}}(\mathbf{U}, A) = \left(q_2, \frac{q_1 q_2}{\eta - b}, \frac{q_2^2}{\eta - b} + \frac{1}{2}g\eta^2 - g(\eta - A)b\right)^\top \ , \tag{28}$$

$$\hat{\mathbf{S}}(\mathbf{U}, A) = (0, -g(\eta - A)b_x - ghf_1, -g(\eta - A)b_y - ghf_2)^\top \ . \tag{29}$$

We consider the scheme satisfied by $\hat{\mathbf{U}}$: find $\hat{\mathbf{U}}^{n+1,C} \in \mathcal{W}_3^{C,k}$ such that $\forall\ \hat{\mathbf{V}} \in \mathcal{W}_3^{C,k}$,

$$\begin{aligned}
\int_{C_{ij}} \hat{\mathbf{U}}^{n+1,C} \cdot \hat{\mathbf{V}} dxdy = &\int_{C_{ij}} \left(\theta \hat{\mathbf{U}}^{n,D} + (1-\theta)\hat{\mathbf{U}}^{n,C}\right) \cdot \hat{\mathbf{V}} dxdy \\
&+\Delta t_n \int_{C_{ij}} \left[\hat{\mathbf{F}}\left(\hat{\mathbf{U}}^{n,D}, A^{n,D}\right) \cdot \hat{\mathbf{V}}_x + \hat{\mathbf{G}}\left(\hat{\mathbf{U}}^{n,D}, A^{n,D}\right) \cdot \hat{\mathbf{V}}_y\right] dxdy \\
&-\Delta t_n \int_{y_{j-\frac{1}{2}}}^{y_{j+\frac{1}{2}}} \left[\hat{\mathbf{F}}\left(\hat{\mathbf{U}}^{n,D}\left(x_{i+\frac{1}{2}}, y\right), A^{n,D}\right) \cdot \hat{\mathbf{V}}\left(x^-_{i+\frac{1}{2}}, y\right)\right. \\
&\left. - \hat{\mathbf{F}}\left(\hat{\mathbf{U}}^{n,D}(x_{i-\frac{1}{2}}, y), A^{n,D}\right) \cdot \hat{\mathbf{V}}\left(x^+_{i-\frac{1}{2}}, y\right)\right] dy \\
&-\Delta t_n \int_{x_{i-\frac{1}{2}}}^{x_{i+\frac{1}{2}}} \left[\hat{\mathbf{G}}\left(\hat{\mathbf{U}}^{n,D}\left(x, y_{j+\frac{1}{2}}\right), A^{n,D}\right) \cdot \hat{\mathbf{V}}\left(x, y^-_{j+\frac{1}{2}}\right)\right. \\
&\left. - \hat{\mathbf{G}}\left(\hat{\mathbf{U}}^{n,D}\left(x, y_{j-\frac{1}{2}}\right), A^{n,D}\right) \cdot \hat{\mathbf{V}}\left(x, y^+_{j-\frac{1}{2}}\right)\right] dx \\
&+\Delta t_n \int_{C_{ij}} \hat{\mathbf{S}}\left(\hat{\mathbf{U}}^{n,D}, A^{n,D}\right) \cdot \hat{\mathbf{V}} dxdy \ .
\end{aligned} \tag{30}$$

The procedure to update $\hat{\mathbf{U}}^{n+1,D}$ is similar to (30), thus it is omitted. Now we suppose the still-water stationary solution $\eta = h + b = C_0$, $u = v = 0$ at $t = 0$, where C_0 is a constant. In the initialization step, it is easy to ensure

$$\hat{\mathbf{U}}^{n,C} = \hat{\mathbf{U}}^{n,D} = (C_0, 0, 0)^\top \ , \tag{31}$$

for $n = 0$.

By induction, assuming condition (31) is true for $n \geq 0$, we want to establish that the numerical solution computed from (30) and its counterpart for $\hat{\mathbf{U}}^{n+1,D}$ satisfy

$$\hat{\mathbf{U}}^{n+1,C} = \hat{\mathbf{U}}^{n+1,D} = (C_0, 0, 0)^\top \ .$$

By virtue of (31),

$$A^{n,D} = C_0, f_1 = f_2 = 0, \tag{32}$$

the first term on the right-hand side of (30) become

$$\int_{C_{ij}} \left(\theta \hat{\mathbf{U}}^{n,D} + (1-\theta)\hat{\mathbf{U}}^{n,C}\right) \cdot \hat{\mathbf{V}} dxdy \quad = \quad \int_{C_{ij}} (C_0, 0, 0)^\top \cdot \hat{\mathbf{V}} dx \ , \tag{33}$$

the flux terms

$$\hat{\mathbf{F}}(\mathbf{U}^{n,D}, A^{n,D}) = \left(0, \frac{1}{2}gC_0^2, 0\right)^\top, \tag{34}$$

$$\hat{\mathbf{G}}(\mathbf{U}^{n,D}, A^{n,D}) = \left(0, 0, \frac{1}{2}gC_0^2\right)^\top, \tag{35}$$

the source term

$$\hat{\mathbf{S}}\left(\mathbf{U}^{n,D}, A^{n,D}\right) = (0,0,0)^\top, \tag{36}$$

With equations (32)-(36) in hand, we have from (30)

$$\begin{aligned}
\int_{C_{ij}} \hat{\mathbf{U}}^{n+1,C} \cdot \hat{\mathbf{V}} dxdy =& \int_{C_{ij}} \left(\theta \hat{\mathbf{U}}^{n,D} + (1-\theta)\hat{\mathbf{U}}^{n,C}\right) \cdot \hat{\mathbf{V}} dxdy \\
&+\Delta t_n \int_{C_{ij}} \left[\hat{\mathbf{F}}\left(\mathbf{U}^{n,D}, A^{n,D}\right) \cdot \hat{\mathbf{V}}_x + \hat{\mathbf{G}}\left(\mathbf{U}^{n,D}, A^{n,D}\right) \cdot \hat{\mathbf{V}}_y\right] dxdy \\
&-\Delta t_n \int_{y_{j-\frac{1}{2}}}^{y_{j+\frac{1}{2}}} \left[\hat{\mathbf{F}}\left(\mathbf{U}^{n,D}\left(x_{i+\frac{1}{2}}, y\right), A^{n,D}\right) \cdot \hat{\mathbf{V}}\left(x^-_{i+\frac{1}{2}}, y\right)\right. \\
&\left. - \hat{\mathbf{F}}\left(\mathbf{U}^{n,D}(x_{i-\frac{1}{2}}, y), A^{n,D}\right) \cdot \hat{\mathbf{V}}\left(x^+_{i-\frac{1}{2}}, y\right)\right] dy \\
&-\Delta t_n \int_{x_{i-\frac{1}{2}}}^{x_{i+\frac{1}{2}}} \left[\hat{\mathbf{G}}\left(\mathbf{U}^{n,D}\left(x, y_{j+\frac{1}{2}}\right), A^{n,D}\right) \cdot \hat{\mathbf{V}}\left(x, y^-_{j+\frac{1}{2}}\right)\right. \\
&\left. - \hat{\mathbf{G}}\left(\mathbf{U}^{n,D}\left(x, y_{j-\frac{1}{2}}\right), A^{n,D}\right) \cdot \hat{\mathbf{V}}\left(x, y^+_{j-\frac{1}{2}}\right)\right] dx \\
&+\Delta t_n \int_{C_{ij}} \hat{\mathbf{S}}\left(\mathbf{U}^{n,D}, A^{n,D}\right) \cdot \hat{\mathbf{V}} dxdy \\
=& \int_{C_{ij}} (C_0, 0, 0)^\top \cdot \hat{\mathbf{V}} dx \\
&+\Delta t_n \int_{C_{ij}} \left[\left(0, \frac{1}{2}gC_0^2, 0\right)^\top \cdot \hat{\mathbf{V}}_x + \left(0, 0, \frac{1}{2}gC_0^2\right)^\top \cdot \hat{\mathbf{V}}_y\right] dxdy \\
&-\Delta t_n \int_{y_{j-\frac{1}{2}}}^{y_{j+\frac{1}{2}}} \left[\left(0, \frac{1}{2}gC_0^2, 0\right)^\top \cdot \hat{\mathbf{V}}\left(x^-_{i+\frac{1}{2}}, y\right)\right. \\
&\left. - \left(0, \frac{1}{2}gC_0^2, 0\right)^\top \cdot \hat{\mathbf{V}}\left(x^+_{i-\frac{1}{2}}, y\right)\right] dy \\
&-\Delta t_n \int_{x_{i-\frac{1}{2}}}^{x_{i+\frac{1}{2}}} \left[\left(0, 0, \frac{1}{2}gC_0^2\right)^\top \cdot \hat{\mathbf{V}}\left(x, y^-_{j+\frac{1}{2}}\right)\right. \\
&\left. - \left(0, 0, \frac{1}{2}gC_0^2\right)^\top \cdot \hat{\mathbf{V}}\left(x, y^+_{j-\frac{1}{2}}\right)\right] dx \\
&+\Delta t_n \int_{C_{ij}} (0,0,0)^\top \cdot \hat{\mathbf{V}} dxdy \\
=& \int_{C_{ij}} (C_0, 0, 0)^\top \cdot \hat{\mathbf{V}} dx
\end{aligned}$$

Equation (**??**) gives

$$\int_{C_{ij}} \left(\hat{\mathbf{U}}^{n+1,C} - (C_0, 0, 0)^\top\right) \cdot \hat{\mathbf{V}} dxdy \quad = \quad 0$$

By further taking $\hat{\mathbf{V}} = \hat{\mathbf{U}}^{n+1,C} - (C_0, 0, 0)^\top$, we obtain

$$\int_{C_{ij}} \left| \hat{\mathbf{U}}^{n+1,C} - (C_0, 0, 0)^\top \right|^2 dxdy \quad = \quad 0$$

and thus $\hat{\mathbf{U}}^{n+1,C} = (C_0, 0, 0)^\top$. Similarly, we can establish $\hat{\mathbf{U}}^{n+1,D} = (C_0, 0, 0)^\top$. This completes the proof.

□

3.4. Non-negativity of the volumetric sediment concentration. Some shallow water flows over erodible beds involve low volumetric sediment concentration which is close to zero or equal to zero. If no special attention is paid, standard numerical methods may produce unacceptable negative value of the volumetric sediment concentration. In this subsection, we discuss the non-negativity of the volumetric sediment concentration.

To do so, we denote $\bar{r}_{ij}^{n,C}$ (resp. $\bar{r}_{ij}^{n,D}$) as the cell average of the solution function $r^{n,C}$ (resp. $r^{n,D}$) over C_{ij} (resp. D_{ij}) at time t_n. The cell average of the numerical solution $r_{ij}^{n+1,C}$ can be obtained by taking the test function $\mathbf{V} = (0, 0, 0, \frac{1}{\Delta x \Delta y}, 0)^\top$ in (24) or (17):

$$\begin{aligned}
\bar{r}_{ij}^{n+1,C} \quad &= \quad (1-\theta)\bar{r}_{ij}^{n,C} + \frac{\theta}{\Delta x \Delta y} \int_{C_{ij}} r^{n,D} dxdy \\
&- \quad \frac{\Delta t_n}{\Delta x \Delta y} \int_{y_{j-\frac{1}{2}}}^{y_{j+\frac{1}{2}}} \left[\frac{q_1^{n,D}\left(x_{i+\frac{1}{2}}, y\right) r^{n,D}\left(x_{i+\frac{1}{2}}, y\right)}{\eta^{n,D}\left(x_{i+\frac{1}{2}}, y\right) - b^{n,D}\left(x_{i+\frac{1}{2}}, y\right)} \right. \\
&- \quad \left. \frac{q_1^{n,D}\left(x_{i-\frac{1}{2}}, y\right) r^{n,D}\left(x_{i-\frac{1}{2}}, y\right)}{\eta^{n,D}\left(x_{i-\frac{1}{2}}, y\right) - b^{n,D}\left(x_{i-\frac{1}{2}}, y\right)} \right] dy \\
&- \quad \frac{\Delta t_n}{\Delta x \Delta y} \int_{x_{i-\frac{1}{2}}}^{x_{i+\frac{1}{2}}} \left[\frac{q_2^{n,D}\left(x, y_{j+\frac{1}{2}}\right) r^{n,D}\left(x, y_{j+\frac{1}{2}}\right)}{\eta^{n,D}\left(x, y_{j+\frac{1}{2}}\right) - b^{n,D}\left(x, y_{j+\frac{1}{2}}\right)} \right. \\
&- \quad \left. \frac{q_2^{n,D}\left(x, y_{j-\frac{1}{2}}\right) r^{n,D}\left(x, y_{j-\frac{1}{2}}\right)}{\eta^{n,D}\left(x, y_{j-\frac{1}{2}}\right) - b^{n,D}\left(x, y_{j-\frac{1}{2}}\right)} \right] dx \\
&+ \quad \frac{\Delta t_n}{\Delta x \Delta y} \int_{C_{ij}} E^{n,D} - M^{n,D} dxdy \\
&= \quad (1-\theta)\bar{r}_{ij}^{n,C} + \frac{\theta}{\Delta x \Delta y} \int_{C_{ij}} r^{n,D} dxdy \\
&- \quad \frac{\Delta t_n}{\Delta x \Delta y} \int_{y_{j-\frac{1}{2}}}^{y_{j+\frac{1}{2}}} \left[u^{n,D}\left(x_{i+\frac{1}{2}}, y\right) r^{n,D}\left(x_{i+\frac{1}{2}}, y\right) \right. \\
&- \quad \left. u^{n,D}\left(x_{i-\frac{1}{2}}, y\right) r^{n,D}\left(x_{i-\frac{1}{2}}, y\right) \right] dy \\
&- \quad \frac{\Delta t_n}{\Delta x \Delta y} \int_{x_{i-\frac{1}{2}}}^{x_{i+\frac{1}{2}}} \left[v^{n,D}\left(x, y_{j+\frac{1}{2}}\right) r^{n,D}\left(x, y_{j+\frac{1}{2}}\right) \right. \\
&- \quad \left. v^{n,D}\left(x, y_{j-\frac{1}{2}}\right) r^{n,D}\left(x, y_{j-\frac{1}{2}}\right) \right] dx \\
&+ \quad \Delta t_n \overline{E}_{C_{ij}}^{n,D} - \frac{\Delta t_n}{\Delta x \Delta y} \int_{C_{ij}} \hat{M}^{n,D} r^{n,D} dxdy,
\end{aligned}$$

where

$$u^{n,D} = \frac{q_1^{n,D}}{\eta^{n,D} - b^{n,D}}, \tag{37}$$

$$v^{n,D} = \frac{q_2^{n,D}}{\eta^{n,D} - b^{n,D}}, \tag{38}$$

$$\overline{E}_{C_{ij}}^{n,D} = \frac{1}{\Delta x \Delta y} \int_{C_{ij}} E^{n,D} dxdy. \tag{39}$$

$$\hat{M} = \frac{M}{r} = \frac{\alpha w_0 (1 - \alpha r/(\eta - b))^m}{\eta - b} \tag{40}$$

In the numerical implementation, the definite integrals in the intervals $[x_{i-\frac{1}{2}}, x_{i+\frac{1}{2}}]$, $[y_{j-\frac{1}{2}}, y_{j+\frac{1}{2}}]$ and cell C_{ij} are usually evaluated by the Gauss quadrature rule. Notice that the numerical solutions are discontinuous along $x = x_i$ or $y = y_j$, the scheme (37) becomes

$$\begin{aligned}
\bar{r}_{ij}^{n+1,C} &= (1-\theta)\bar{r}_{ij}^{n,C} + \frac{\theta}{\Delta x \Delta y} \int_{C_{ij}} r^{n,D} dxdy \\
&- \frac{\Delta t_n}{2\Delta x} \sum_{s=1}^{2} \sum_{\gamma=1}^{N} \omega_\gamma \Big[u^{n,D}\left(\hat{x}_i^{2,\hat{N}}, y_j^{s,\gamma}\right) r^{n,D}\left(\hat{x}_i^{2,\hat{N}}, y_j^{s,\gamma}\right) \\
&- u^{n,D}\left(\hat{x}_i^{1,1}, y_j^{s,\gamma}\right) r^{n,D}\left(\hat{x}_i^{1,1}, y_j^{s,\gamma}\right) \Big] \\
&- \frac{\Delta t_n}{2\Delta y} \sum_{l=1}^{2} \sum_{\beta=1}^{N} \omega_\beta \Big[v^{n,D}\left(x_i^{l,\beta}, \hat{y}_j^{2,\hat{N}}\right) r^{n,D}\left(x_i^{l,\beta}, \hat{y}_j^{2,\hat{N}}\right) \\
&- v^{n,D}\left(x_i^{l,\beta}, \hat{y}_j^{1,1}\right) r^{n,D}\left(x_i^{l,\beta}, \hat{y}_j^{1,1}\right) \Big] + \Delta t_n \overline{E}_{C_{ij}}^{n,D} \\
&- \frac{\Delta t_n}{4} \sum_{l,s=1}^{2} \sum_{\beta,\gamma=1}^{N} \omega_\beta \omega_\gamma \hat{M}^{n,D}\left(x_i^{l,\beta}, y_j^{s,\gamma}\right) r^{n,D}\left(x_i^{l,\beta}, y_j^{s,\gamma}\right),
\end{aligned} \tag{41}$$

herein, we used $\hat{x}_i^{1,1} = x_{i-\frac{1}{2}}, \hat{x}_i^{2,\hat{N}} = x_{i+\frac{1}{2}}, \hat{y}_j^{1,1} = y_{j-\frac{1}{2}}, \hat{y}_j^{2,\hat{N}} = y_{j+\frac{1}{2}}$. The evaluation of $\overline{E}_{C_{ij}}^{n,D}$ defined in (39) is also given by Gauss quadrature rule.

Since the numerical solution $r^{n,D}$ is a piecewise polynomial with degree $k+1$, the first integral in cell C_{ij} in (41) is exactly evaluated by using the Gauss quadrature rule in our numerical implementation. However, in order to discuss the non-negativity of the volumetric sediment concentration r. We here calculate the integral using a combination of the Gauss quadrature rule and the Legendre Gauss-Lobatto quadrature rule as follows:

$$\begin{aligned}
\frac{\theta}{\Delta x \Delta y} \int_{C_{ij}} r^{n,D} dxdy &= \frac{\theta}{3\Delta x \Delta y} \int_{C_{ij}} r^{n,D} dxdy \\
&+ \frac{\theta}{3\Delta x \Delta y} \int_{C_{ij}} r^{n,D} dxdy + \frac{\theta}{3\Delta x \Delta y} \int_{C_{ij}} r^{n,D} dxdy \\
&= \frac{\theta}{3} \sum_{l,s=1}^{2} \sum_{\beta,\gamma=1}^{N} \omega_\beta \omega_\gamma r^{n,D}\left(x_i^{l,\beta}, y_j^{s,\gamma}\right) \\
&+ \frac{\theta}{3} \sum_{l,s=1}^{2} \sum_{\beta=1}^{N} \sum_{\gamma=1}^{\hat{N}} \omega_\beta \hat{\omega}_\gamma r^{n,D}\left(x_i^{l,\beta}, \hat{y}_j^{s,\gamma}\right) \\
&+ \frac{\theta}{3} \sum_{l,s=1}^{2} \sum_{\beta=1}^{\hat{N}} \sum_{\gamma=1}^{N} \hat{\omega}_\beta \omega_\gamma r^{n,D}\left(\hat{x}_i^{l,\beta}, y_j^{s,\gamma}\right).
\end{aligned} \tag{42}$$

Plugging (42) into (41), one obtains

$$
\begin{aligned}
\bar{r}_{ij}^{n+1,C} &= (1-\theta)\bar{r}_{ij}^{n,C} + \Delta t_n \overline{E}_{C_{ij}}^{n,D} \\
&+ \sum_{s=1}^{2}\sum_{\gamma=1}^{N}\omega_\gamma\left[\frac{\theta}{3}\hat{\omega}_1 - \frac{\Delta t_n}{2\Delta x}u^{n,D}\left(\hat{x}_i^{2,\hat{N}}, y_j^{s,\gamma}\right)\right] r^{n,D}\left(\hat{x}_i^{2,\hat{N}}, y_j^{s,\gamma}\right) \\
&+ \sum_{s=1}^{2}\sum_{\gamma=1}^{N}\omega_\gamma\left[\frac{\theta}{3}\hat{\omega}_1 + \frac{\Delta t_n}{2\Delta x}u^{n,D}\left(\hat{x}_i^{1,1}, y_j^{s,\gamma}\right)\right] r^{n,D}\left(\hat{x}_i^{1,1}, y_j^{s,\gamma}\right) \\
&+ \sum_{l=1}^{2}\sum_{\beta=1}^{N}\omega_\beta\left[\frac{\theta}{3}\hat{\omega}_1 - \frac{\Delta t_n}{2\Delta y}v^{n,D}\left(x_i^{l,\beta}, \hat{y}_j^{2,\hat{N}}\right)\right] r^{n,D}\left(x_i^{l,\beta}, \hat{y}_j^{2,\hat{N}}\right) \\
&+ \sum_{l=1}^{2}\sum_{\beta=1}^{N}\omega_\beta\left[\frac{\theta}{3}\hat{\omega}_1 + \frac{\Delta t_n}{2\Delta y}v^{n,D}\left(x_i^{l,\beta}, \hat{y}_j^{1,1}\right)\right] r^{n,D}\left(x_i^{l,\beta}, \hat{y}_j^{1,1}\right) \\
&+ \sum_{l,s=1}^{2}\sum_{\beta,\gamma=1}^{N}\omega_\beta\omega_\gamma\left[\frac{\theta}{3} - \frac{\Delta t_n}{4}\hat{M}^{n,D}\left(x_i^{l,\beta}, y_j^{s,\gamma}\right)\right] r^{n,D}\left(x_i^{l,\beta}, y_j^{s,\gamma}\right) \\
&+ \frac{\theta}{3}\sum_{l,s=1}^{2}\sum_{\beta=2}^{\hat{N}-1}\sum_{\gamma=1}^{N}\hat{\omega}_\beta\omega_\gamma r^{n,D}\left(\hat{x}_i^{l,\beta}, y_j^{s,\gamma}\right) \\
&+ \frac{\theta}{3}\sum_{s=1}^{2}\sum_{\gamma=1}^{N}\omega_\gamma\hat{\omega}_1\left(r^{n,D}\left(\hat{x}_i^{2,1}, y_j^{s,\gamma}\right) + r^{n,D}\left(\hat{x}_i^{1,\hat{N}}, y_j^{s,\gamma}\right)\right) \\
&+ \frac{\theta}{3}\sum_{l,s=1}^{2}\sum_{\beta=1}^{N}\sum_{\gamma=2}^{\hat{N}-1}\omega_\beta\hat{\omega}_\gamma r^{n,D}\left(x_i^{l,\beta}, \hat{y}_j^{s,\gamma}\right) \\
&+ \frac{\theta}{3}\sum_{l=1}^{2}\sum_{\beta=1}^{N}\omega_\beta\hat{\omega}_1\left(r^{n,D}\left(x_i^{l,\beta}, \hat{y}_j^{2,1}\right) + r^{n,D}\left(x_i^{l,\beta}, \hat{y}_j^{1,\hat{N}}\right)\right). \qquad (43)
\end{aligned}
$$

Here, we used $\hat{\omega}_{\hat{N}} = \hat{\omega}_1$. Now, we have the following theorem from (43).

Theorem 2. *For any given $n \geq 0$, we assume $\bar{r}_{ij}^{n,C} \geq 0$ and $\bar{r}_{ij}^{n,D} \geq 0$, $\forall i,j$. Consider the numerical scheme in (41) and its counterpart for $\bar{r}_{ij}^{n+1,D}$, if $r^{n,C}(x,y) \geq 0$, $r^{n,D}(x,y) \geq 0$, $\forall (x,y) \in L_{i,j}^{l,m}$, $\forall i,j$ with $l,m = 1,2$, then $\bar{r}_{ij}^{n+1,C} \geq 0$ and $\bar{r}_{ij}^{n+1,D} \geq 0$, $\forall i,j$, provided that the time step Δt_n satisfies*

$$\Delta t_n \leq \min\left(\frac{2\theta\widehat{\omega}_1\Delta x}{3a_x}, \ \frac{2\theta\widehat{\omega}_1\Delta y}{3a_y}, \ \frac{4\theta}{3\hat{d}}\right) \qquad (44)$$

where $\hat{d} = \max\left(\|\hat{M}^{n,C}\|_\infty, \|\hat{M}^{n,D}\|_\infty\right)$, $a_x = \max\left(\|u^{n,C}\|_\infty, \|u^{n,D}\|_\infty\right)$ and $a_y = \max\left(\|v^{n,C}\|_\infty, \|v^{n,D}\|_\infty\right)$.

Since a source term appearing in the sediment transport equation, the CFL condition is different from the one in [22], in which the positivity-preserving scheme was designed for the water depth.

Finally, to satisfy the sufficient condition given in Theorem 2, a positivity-preserving limiter is employed to modify the numerical solutions $r^{n,C}$ and $r^{n,D}$ which is the same as the one applied to the water depth in [37, 22]. Let K denote an element from the primal mesh or the dual mesh and $\widehat{L}_K$ represent the set of relevant quadrature points in K, namely on the primal mesh $K = C_{ij}$, $\widehat{L}_K = \cup_{l,m=1}^{2} L_{i,j}^{l,m}$ and on the dual mesh $K = D_{ij}$, $\widehat{L}_K = L_{i,j}^{1,1} \cup L_{i,j-1}^{1,2} \cup L_{i-1,j}^{2,1} \cup L_{i-1,j-1}^{2,2}$. The positivity-preserving limiter is given as follows: on each mesh element K, we modify the water depth $r^{n,\star}$ ($\star = C, D$) into $\widetilde{r}^{n,\star} = \beta_K(r^{n,\star} - \bar{r}^{n,\star}) + \bar{r}^{n,\star}$ with

$$\beta_K = \min_{x \in \widehat{L}_K}\left\{1, \left|\frac{\bar{r}^{n,\star}}{\bar{r}^{n,\star} - r^{n,\star}(x)}\right|\right\}.$$

3.5. High-order time discretization. So far, the scheme is proposed when the first order forward Euler method is taken as the time discretization. To achieve better accuracy in time, a third-order TVD Runge-Kutta scheme is employed for time discretization [9]. Such discretization can be written as a convex combination of the forward Euler method, and therefore the resulting scheme is still well-balanced and can maintain the non-negativity of the volumetric sediment concentration. The time step restriction for the third order TVD Runge-Kutta scheme is the same as the one for the forward Euler method.

3.6. Summary of the proposed scheme. Finally, we summarize the complete procedure of the well-balanced and positivity-preserving central DG method for the fully coupled shallow water equations over erodible bed:

1. Compute the initial data $\mathbf{U}^{0,C}$ and $\mathbf{U}^{0,D}$, set $n := 0$.
2. Compute the time step Δt_n according to Theorem 2.
3. Apply the positivity-preserving limiter in Section 3.4 to modify the numerical solutions $r^{n,C}$ and $r^{n,D}$ into $\widetilde{r}^{n,C}$ and $\widetilde{r}^{n,D}$, then redefine $\mathbf{U}^{n,C} = (\eta^{n,C}, q_1^{n,C}, q_2^{n,C}, \widetilde{r}^{n,C}, b^{n,C})^\top$ and $\mathbf{U}^{n,D} = (\eta^{n,D}, q_1^{n,D}, q_2^{n,D}, \widetilde{r}^{n,D}, b^{n,D})^\top$.
4. Apply the well-balanced central DG method (24) to update the solutions $\mathbf{U}^{n+1,C}$ and $\mathbf{U}^{n+1,D}$
5. Set $n := n + 1$, goto 2.

Remark 1. *In the final numerical implementation, the third order TVD Runge-Kutta method is used to advance the time and thus the positivity-preserving limiter is applied to modify the numerical solutions of r at each inner stage of the Runge-Kutta method.*

4. Numerical examples

In this section, numerical experiments are presented to demonstrate the performance of the proposed method for solving the fully coupled 2D system of the SW equations and the sediment transport equations. All simulations are performed with P^2 approximations, and all reported results are from numerical solutions on the primal mesh. In all simulations, we use a uniform mesh with constant mesh sizes Δx and Δy in the x- and y-directions, respectively. We set $\theta = 1$, the kinematic viscosity of water $\nu = 1.2 \times 10^{-6}$, the Manning's roughness coefficient $n_b = 0.02$, the parameters $\phi = 0.015$, $\gamma_c = 0.047$ and $m = 2$. In this computation, we use the total variation bounded (TVB) minmod slope limiter [9] to prevent numerical instabilities. It is used prior to application of the positivity-preserving limiter.

4.1. Well-balanced test. In this test, we validate the well-balanced feature of the proposed method as applied to a quiescent water with uniform sediment deposition. The initial conditions are

$$\begin{aligned} \eta(x,y,0) &= 1 , \\ u(x,y,0) &= v(x,y,0) = 0 , \\ b(x,y,0) &= 0 , \\ c(x,y,0) &= 0.7e^{-5(x-0.9)^2-50(y-0.5)^2} , \end{aligned}$$

In this test, we set the gravitational constant $g = 9.8$, the bed porosity $p = 0.28$, the sediment diameter $d = 0.01$, the density of sediment particles $\rho_s = 2400$, the density of water $\rho_f = 1000$, and the coefficient $\mu = 0$ in equation (5).

We choose $[-1, 3] \times [-0.5, 1.5]$ as the computational domain, divided into 40×20 elements, and use the outgoing boundary conditions for all boundaries. We compute the solution up to $t = 100$ by the proposed method.

We implement the computation in both single and double precision. The corresponding L^∞ errors on the water surface η, discharges hu and hv are given in Table 1. It can be seen from this table that these values have orders of magnitude consistent with machine precision, thus the proposed scheme preserves the "still-water" solution exactly. Besides,

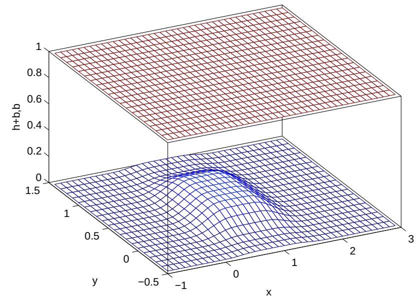

FIGURE 2. Numerical results (free surface $h+b$ and bottom b) for the stationary solution at $t = 100$.

we also plot the water surface and the bed profile at $t = 100$ in Figure 2. It can be observed from this figure that there are no oscillations developed at the water surface during the evolution of a variable bed.

TABLE 1. L^∞ errors on (η, hu, hv) for the stationary solution at $t = 100$.

precision	η	hu	hv
single	1.32E-07	3.23E-08	3.72E-08
double	5.65E-14	2.73E-15	3.25E-15

4.2. Positivity-preserving test. In this test, we investigate the non-negativity of the volumetric sediment concentration c by the proposed method. We consider a dam break problem over an erodible bed with the initial conditions:

$$\begin{aligned}
\eta(x,y,0) &= \begin{cases} 2\ , & x \le 1\ , \\ 1\ , & \text{otherwise}\ , \end{cases} \\
u(x,y,0) &= v(x,y,0) \ = \ 0\ , \\
c(x,y,0) &= 0.0\ , \\
b(x,y,0) &= 0.7e^{-5(x-0.9)^2-50(y-0.5)^2}\ ,
\end{aligned}$$

In this test, we set the gravitational constant $g = 9.8$, the bed porosity $p = 0.28$, the sediment diameter $d = 0.01$, the density of sediment particles $\rho_s = 2400$, the density of water $\rho_f = 1000$, and the coefficient $\mu = 0$ in equation (5).

The computational domain $[-1, 3] \times [-0.5, 1.5]$, divided into 80×40 uniform cells, and the outgoing boundary conditions are used for all boundaries. We compute the solution at $t = 0.2$ and 0.5 by the proposed method with or without positivity-preserving limiter (PPL). For a comparison, we use same CFL number (0.1) for both tests. We show the numerical water surface $h+b$ obtained by both methods in Figure 3, the results match well with each other. However, the volumetric sediment concentration c is equal to zero at the initial time and then gradually increases as the time goes. Without the use of the algorithm presented in section 3.4, the simulation produces non-physical numerical solution for the volumetric sediment concentration (See Figure 4). By using the algorithm presented in section 3.4, the numerical volumetric sediment concentration c is always non-negative.

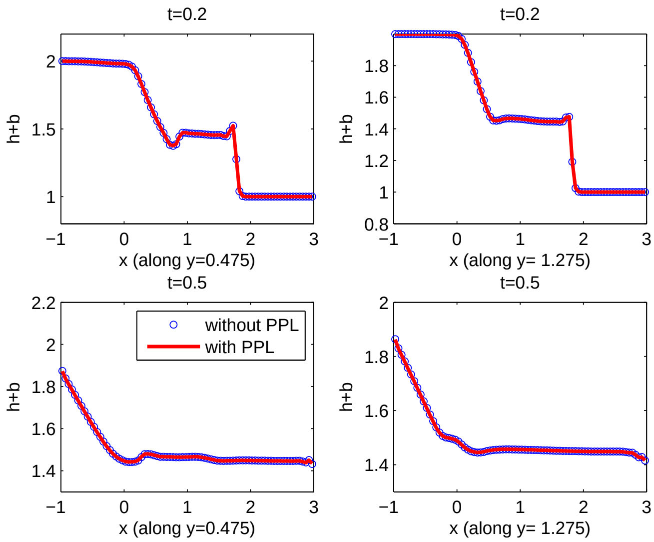

FIGURE 3. Numerical water surface $\eta = h + b$ for the positivity-preserving test at $t = 0.2$ and 0.5.

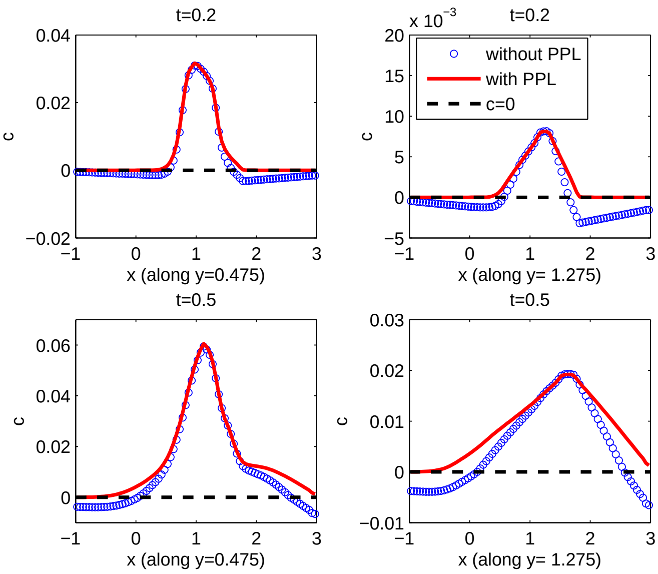

FIGURE 4. Numerical volumetric sediment concentration c for the positivity-preserving test at $t = 0.2$ and 0.5.

4.3. Perturbation of a stationary solution. We next consider a perturbation to a "still-water" state [27]. The initial conditions are given by

$$\begin{aligned}
\eta(x, y, 0) &= \begin{cases} 1 + \varepsilon\,, & 0.05 \le x \le 0.15\,, \\ 1\,, & \text{otherwise}\,, \end{cases} \\
u(x, y, 0) &= v(x, y, 0) = 0\,, \\
c(x, y, 0) &= 0.05\,, \\
b(x, y, 0) &= 0.8\, e^{-5(x-0.9)^2 - 50(y-0.5)^2}\,.
\end{aligned}$$

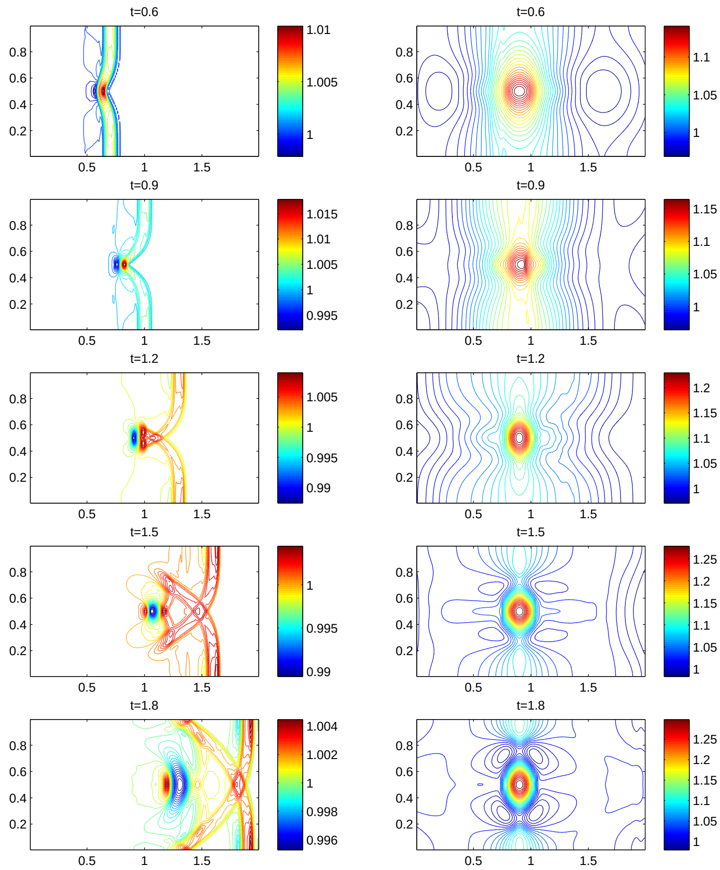

FIGURE 5. Contours of the surface level $h+b$ for the perturbation of a stationary solution at $t = 0.6$, 0.9, 1.2, 1.5 and 1.8. Left: well-balanced central DG method, right: standard central DG method.

where ε is a non-zero perturbation parameter. In this test, we set the perturbation $\varepsilon = 0.01$, the gravitational constant $g = 1$, the bed porosity $p = 0.3$, the sediment diameter $d = 0.01$, the density of sediment particles $\rho_s = 2.4$, the density of water $\rho_f = 1$, and the coefficient $\mu = 0.001$ in equation (5), we also choose $w_0 = 1$ instead of (10).

The computational domain is $[0, 2] \times [0, 1]$. The well-balanced central DG method is used to solve this problem on a 200×100 mesh. The left column in Figure 5 displays the water surface $h + b$ at $t = 0.6$, 0.9, 1.2, 1.5 and 1.8. Clearly, we can see that the numerical solution is able to capture complex small features of the flow as reported in [27]. To demonstrate the importance of the well-balanced property, we also compare with numerical results by the standard central DG method for the same mesh, as presented in the right column of Figure 5. The numerical solutions exhibit spurious oscillations of large amplitude. We also used a smaller perturbation $\varepsilon = 0.0001$ to test the well-balanced property of the presented method, similar results have been observed, and thus they are not shown here. Besides, in Figure 6 we also show a comparison between the central upwind scheme on 20658 triangular cells in [27] and the well-balanced central DG method on a coarser grid (100×50 rectangular cells). It can be seen from this figure that the results from the well-balanced central DG method are comparable to the results from the central upwind scheme in [27].

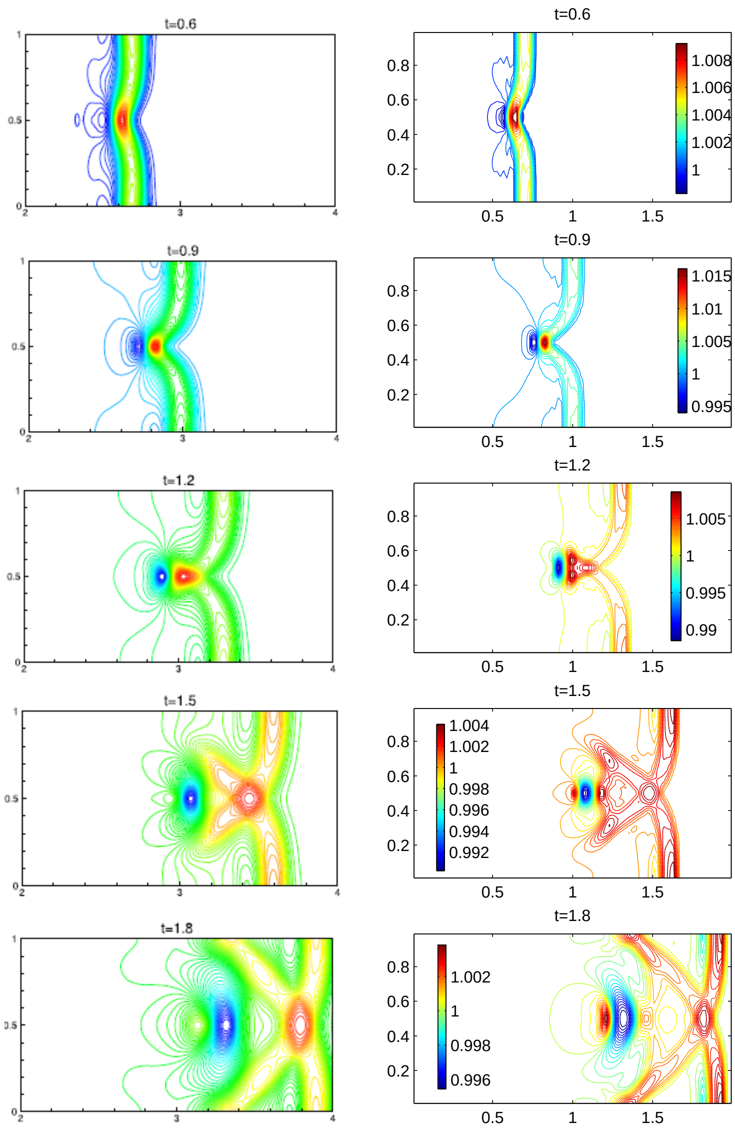

FIGURE 6. Comparison between the central upwind scheme (20658 triangular cells) and the well-balanced central DG method (100×50 rectangular cells) for the perturbation of a stationary solution at $t = 0.6,\ 0.9,\ 1.2,\ 1.5$ and 1.8. Left: central upwind scheme [27], right: well-balanced central DG method.

4.4. Dam-break problem in a long channel over erodible bed. In this test, we study a dam-break flow in a long channel over erodible beds to verify the well-balanced property of the proposed method. The initial conditions are

$$\begin{aligned} \eta(x,y,0) &= \begin{cases} 3.1\ , & x \le 20\ , \\ 0.2\ , & \text{otherwise}\ , \end{cases} \\ u(x,y,0) &= v(x,y,0) = 0\ , \\ c(x,y,0) &= b(x,y,0) = 0\ . \end{aligned}$$

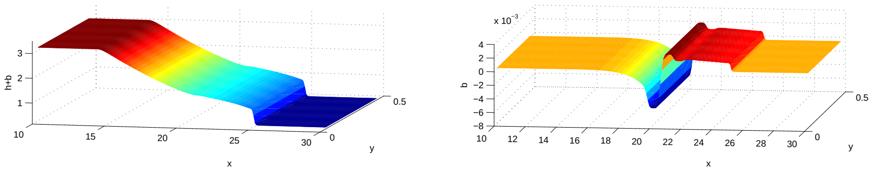

FIGURE 7. Numerical results for dam-break problem in a long channel over erodible bed at $t = 1$.

In the simulation, we neglect the sediment entrainment effects so that we set $E = D = 0$. The parameter values are $g = 9.8$, $p = 0.28$ and $\mu = 0.001$. The computational domain is $[0, 40] \times [0, 0.5]$ divided into 400×5 uniform cells.

In Figure 7, we show the numerical surface level $h+b$ and bed profile b at $t = 1$. As one can clearly see, even under a high-energetic flow considered in this example, the proposed method produces a stable bed erosion process, and the surface level and the bed profile are physically expectable.

4.5. Dam-break experiment over a movable bed. In this test, we further investigate a dam-break problem over a movable bed which has been studied numerically and experimentally [24, 4].

The initial conditions are

$$\begin{aligned} h(x,y,0) &= \begin{cases} 0.1\,, & x \le 0\,, \\ 0.0\,, & \text{otherwise}\,, \end{cases} \\ u(x,y,0) &= v(x,y,0) \;=\; 0\,, \\ c(x,y,0) &= 0\,. \\ b(x,y,0) &= 0\,. \end{aligned}$$

In the simulation, the computational domain is $[-0.6, 0.6] \times [0, 0.2]$ divided into 120×20 uniform cells. The parameter values are $g = 9.8$, $p = 0.28$ and $\mu = 0.0$. The numerical water surface and the bed are shown in Figure 8, which are compared with the observed results in [24, 4]. It can be seen from this figure that the numerical results are agreement with the observed results qualitatively. However, there are obvious differences between these results quantitatively, therefore improving the mathematical model will be a future work.

4.6. Partial dam-break problem over mobile bed. In this numerical test, we simulate a partial dam-break problem with rapidly varying unsteady flow over a mobile bed, which has been investigated in [35, 27].

The initial conditions are

$$\begin{aligned} \eta(x,y,0) &= \begin{cases} 6.8\,, & x \le 95\,, \\ 1\,, & x \ge 105\,, \end{cases} \\ u(x,y,0) &= v(x,y,0) \;=\; 0\,, \\ c(x,y,0) &= b(x,y,0) \;=\; 0\,. \end{aligned}$$

In the simulation, we set $g = 9.8$, $p = 0.28$, $\rho_s = 2400$, $\rho_f = 1000$ and $\mu = 0.001$. The domain $[0, 200] \times [0, 200]$ contains a rectangular dam located in $[95, 105] \times [0, 200]$. The mesh size is $\Delta x = \Delta y = 1$. At initial time $t = 0$, the dam at $[95, 105] \times [85, 160]$ is assumed to break instantaneously and the water starts flowing through the breach. The outgoing boundary condition is used at right boundary and the solid wall boundary conditions are used at all other boundaries.

In Figure 9, we show the numerical surface level $h+b$, the volumetric sediment concentration c and the bed profile b at $t = 8$. As one can clearly see, there is no oscillations and negative values of the volumetric sediment concentration observed. The numerical results are also similar to the one in [27].

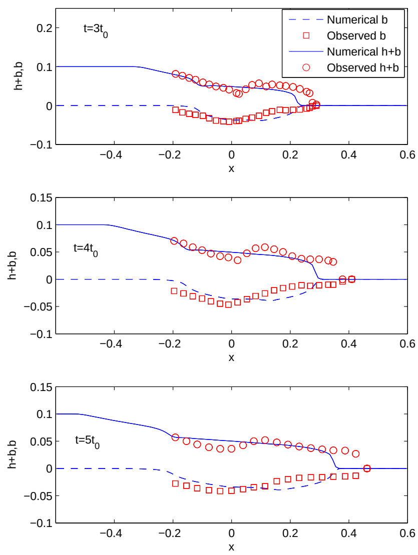

FIGURE 8. Comparison between the numerical results (along $y = 0.1$) and the observed results (Taibei experiment in [24, 4]) for the dam-break problem over a movable bed at $t = 3t_0, 4t_0$ and $5t_0$ with $t_0 = 0.101$.

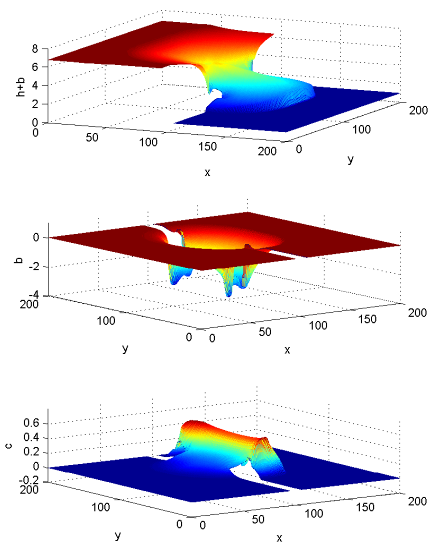

FIGURE 9. Numerical results for partial dam-break problem over mobile bed at $t = 8$.

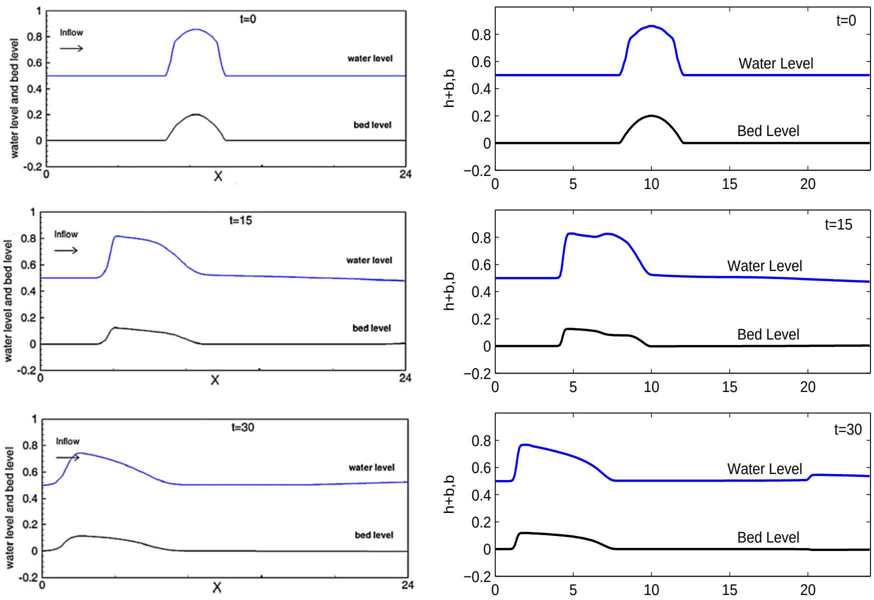

FIGURE 10. Numerical results for the 1D anti-dune problem.

4.7. Anti-dune evolution. In the last test, we consider an anti-dune evolution in 1D space. The initial data is given by

$$\begin{aligned} b(x,0) &= \begin{cases} 0.2 - 0.05(x-10)^2 \ , & 8 \le x \le 12 \ , \\ 0 \ , & \text{otherwise} \ , \end{cases} \\ q(x,0) &= hu(x,0) = q_0 = 1.7 \ . \end{aligned}$$

The water depth $h(x,0)$ is the stationary supercritical profile obtained by the Bernoulli's law

$$\begin{cases} q(x,t) = q_0 \ , \\ \frac{q_0^2}{2gh^2} + h + b = H_0 \ , \end{cases}$$

with $H_0 = \frac{q_0^2}{2gh_0^2} + h_0 + b(0,0)$ and $h_0 = 0.5$. In the test, the computational domain is $[0,24]$ with 240 uniform cells, $\frac{\mu}{1-p} = 0.001$, $g = 9.8$, $E = D = 0$. An inflow boundary condition is used for the water depth $h(0,t) = h_0$ and outflow boundary conditions are used for other variables. The numerical solutions of water level $h+b$ and bed b at $t = 0, 15, 30$ are shown in Figure 10, the results are also compared with the results from the central upwind scheme in [27]. Main features of the anti-dune phenomenon are captured by the well-balanced central DG method. It demonstrates that the well-balanced central DG method can simulate the anti-dune phenomenon.

5. Conclusions

In this work, we have developed a robust numerical method for simulating the shallow water flows over erodible beds. The proposed method is a well-balanced scheme and can maintain the non-negativity of the volumetric sediment concentration in the sediment transport equation. Due to a source term appearing in the sediment transport equation, the constraint to the time step is different to the one in [22], in which the non-negativity of the water depth was considered under the framework of central DG scheme. Although the non-negativity of the water depth is not considered in the present work, it is a trivial work to combine the positivity-preserving scheme to deal with the wetting and drying in [22] into the present work. The present work is built on structured meshes, designing central DG methods with such features on unstructured meshes [20] is envisioned for future work.

Acknowledgments

The work of Yongping Cheng is partially supported by the Chongqing University 2016 "Graduate Student Research Innovation Project" (Project No. CYB16042). The work of Haiyun Dong is partially supported by the NSFC (Grant Nos. 11701055, 11871139).

References

[1] K. Abderrezzak, A. Paquier, B. Gay, One-dimensional numerical modelling of dam-break waves over movable beds: application to experimental and field cases, Environmental Fluid Mechanics, 8 (2008) 169-198.

[2] F. Benkhaldoun, I. Elmahi, S. Sari, M. Seaïd, A two-dimensional finite volume solution of dam-break hydraulics over erodible sediment beds, in: Finite Volumes for Complex Applications. VI. Problems & Perspectives. Vols. 1, 2, in: Springer Proc. Math., vol. 4, Springer, Heidelberg, 2011, pp. 875-891.

[3] Z. Cao, G. Pender, S. Wallis, P. Carling, Computational dam-break hydraulics over erodible sediment bed, Journal of Hydraulic Engineering, 128(5) (2002) 460-472.

[4] H. Capart, D. L. Young, Formation of a jump by the dam-break wave over a granular bed, Journal of Fluid Mechanics, 372 (1998) 165-187.

[5] M. J. Castro Díaz, E. D. Fernández-Nieto, A. M. Ferreiro, Sediment transport models in shallow water equations and numerical approach by high order finite volume methods, Computers & Fluids, 37(3) (2008) 299-316.

[6] A. Canestrelli, M. Dumbser, A. Siviglia, E. F. Toro, Well-balanced high-order centered schemes on unstructured meshes for shallow water equations with fixed and mobile bed, Advances in Water Resources, 33(3) (2010) 291-303.

[7] A. Chen, M. Li, A modified central discontinuous Galerkin method with positivity-preserving and well-balanced properties for the one-dimensional nonlinear shallow water equations, Journal of Computational and Applied Mathematics 345 (2019) 374-387.

[8] Y. Chen, Y. Luo, M. Feng, Analysis of a discontinuous Galerkin method for the Biot's consolidation problem, Applied Mathematics and Computation, 219 (2013) 9043-9056.

[9] B. Cockburn, C.-W. Shu, The Runge-Kutta discontinuous Galerkin method for conservation laws V Multidimensional systems, Journal of Computational Physics, 141 (1998) 199-224 .

[10] H. Dong, M. Li, A reconstructed central discontinuous Galerkin-finite element method for the fully nonlinear weakly dispersive Green-Naghdi model, Applied Numerical Mathematics, 110 (2016) 110?27.

[11] S. Fagherazzi, T. Sun, Numerical simulations of transportational cyclic steps, Computers & Geosciences, 29 (2003) 1143-1154.

[12] S. Gottlieb, C.-W. Shu, E. Tadmor, Strong stability preserving high order time discretization methods, SIAM Review, 43 (2001) 89-112.

[13] P. Hu, Z. Cao, G. Pender, G. Tan, Numerical modelling of turbidity currents in the Xiaolangdi reservoir, Yellow River, China, Journal of Hydrology, 464-465 (2012) 41-53.

[14] E. J. Kubatko, J. J. Westerink, C. Dawson, An unstructured grid morphodynamic model with a discontinuous Galerkin method for bed evolution, Ocean Modelling 15 (2006) 71-89.

[15] A. Kurganov, D. Levy, Central-upwind schemes for the Saint-Venant system, ESAIM Mathematical Modelling and Numerical Analysis, 36 (2002) 397-425.

[16] N. Izem, M. Seaid, I. Elmahi, M. Wakrim, Discontinuous Galerkin method for two-dimensional bilayer shallow water equations, Journal of Engineering Mathematics 96 (2016) 1-21.

[17] D. Lannes, The Water Waves Problem: Mathematical Analysis and Asymptotics, American Mathematical Society, Providence, Rhode Island, 2013.

[18] F. Li, L. Xu, Arbitrary order exactly divergence-free central discontinuous Galerkin methods for ideal MHD equations, Journal of Computational Physics, 231 (2012) 2655-2675.

[19] F. Li, L. Xu, S. Yakovlev, Central discontinuous Galerkin methods for ideal MHD equations with exactly divergence-free magnetic field, Journal of Computational Physics, 230 (2011) 4828-4847.

[20] M. Li, H. Dong, B. Hu, L. Xu, Maximum-principle-satisfying and positivity-preserving high order central DG methods on unstructured overlapping meshes for two-dimensional hyperbolic conservation laws, Journal of Scientific Computing, 79 (2019) 1361-1388.

[21] M. Li, P. Guyenne, F. Li, L. Xu, High order well-balanced CDG-FE methods for shallow water waves by a Green-Naghdi model, Journal of Computational Physics, 257 (2014) 169-192.

[22] M. Li, P. Guyenne, F. Li, L. Xu. A positivity-preserving well-balanced central discontinuous Galerkin methods for the nonlinear shallow water equations, Journal of Scientific Computing, 71 (2017) 994-1034.

[23] M. Li, F. Li, Z. Li, L. Xu. Maximum-principle-satisfying and positivity-preserving high order central discontinuous Galerkin methods for hyperbolic conservation laws, SIAM Journal on Scientific Computing, 38 (2016) A3720-A3740.

[24] S. Li, C. J. Duffy, Fully coupled approach to modeling shallow water flow, sediment transport, and bed evolution in rivers, Water Resources Research, 47(3) (2011) W03508.

[25] Q. Liang, F. Marche, Numerical resolution of well-balanced shallow water equations with complex source terms, Advances in Water Resources, 32 (2009) 873?84.

[26] Y. Liu, C.-W. Shu, E. Tadmor, M. Zhang, Central discontinuous Galerkin methods on overlapping cells with a nonoscillatary hierarchical reconstruction, SIAM Journal on Numerical Analysis, 45 (2007) 2442-2467.

[27] X. Liu, A. Mohammadian, A. Kurganov, J. A. Infante Sedano, Well-balanced central-upwind scheme for a fully coupled shallow water system modeling flows over erodible bed, Journal of Computational Physics, 300 (2015) 202-218.

[28] Y. Luo, M. Feng, Y. Xu, A stabilized mixed discontinuous Galerkin method for the incompressible miscible displacement problem, Boundary Value Problems, 2011 (2011) 48.

[29] J. Murillo, P. Garcia-Navarro, An Exner-based coupled model for two-dimensional transient flow over erodible bed, Journal of Computational Physics, 229(23) (2010) 8704-8732.

[30] D. Pritchard, A. J. Hogg, On sediment transport under dam-break flow, Journal of Fluid Mechanics, 473 (2002) 265-274.

[31] T. Rowana, M. Seaidb, Two-dimensional numerical modelling of shallow water flows over multilayer movable beds, Applied Mathematical Modelling 88 (2020) 474-497.

[32] G. Simpson, S. Castelltort, Coupled model of surface water flow, sediment transport and morphological evolution, Computers & Geosciences, 32(10) (2006) 1600-1614.

[33] P. A. Tassi, S. Rhebergen, C. A. Vionnet, O. Bokhove, A discontinuous Galerkin finite element model for river bed evolution under shallow flows, Computer Methods in Applied Mechanics and Engineering, 197(33-40) (2008) 2930-2947.

[34] T. Tingsanchali, C. Chinnarasri, Numerical modelling of dam failure due to flow overtopping, Hydrological Sciences Journal, 46(1) (2001) 113-130.

[35] J. Xia, B. Lin, R. A. Falconer, G. Wang, Modelling dam-break flows over mobile beds using a 2D coupled approach, Advances in Water Resources, 33(2) (2010) 171-183.

[36] Y. Xing, C.-W. Shu, High order finite difference WENO schemes with the exact conservation property for the shallow water equations, Journal of Computational Physics, 208 (2005) 206-227.

[37] Y. Xing, X. Zhang, C.-W. Shu, Positivity-preserving high order well-balanced discontinuous Galerkin methods for the shallow water equations. Advances in Water Resources, 33 (2010) 1476-1493.

[38] Z. Xu, Y. Liu, New central and central discontinuous Galerkin schemes on overlapping cells of unstructured grids for solving ideal magnetohydrodynamic equations with globally divergence-free magnetic field, Journal of Computational Physics, 327 (2016) 203-224.

[39] Z.Y. Yue, Z.X. Cao, X. Li, T. Che, Two-dimensional coupled mathematical modeling of fluvial processes with intense sediment transport and rapid bed evolution, Science in China Series G: Physics, Mechanics and Astronomy, 51(9) (2008) 1427-1438.

College of Computer Science, Chongqing University, Chongqing, 400044, P.R. China
E-mail: `wasxxwz@163.com`

School of arts and sciences, Chengdu College of University of Electronic Science and Technology of China, Chengdu, 611731, P.R. China
E-mail: `chenam2007@126.com`

College of Mathematics and Statistics, Chongqing University, Chongqing, 401331, P.R. China
E-mail: `cyp@cqu.edu.cn and dhy@cqu.edu.cn`